photoemission is observed. By contrast, at 400 nm only decay of the laser-induced excess concentration occurred. A model is suggested to explain the results based on competition between trap-filling and thermal decay. The refilling of empty traps by the photoexcited electrons is probably through the p-band at 600 nm and through the conduction band or a higher energy band at 400 nm. It is not possible from these results to calculate the density of trapped electrons, but other studies suggest that the concentrations are less than a few percent of the Na^- concentration.

These studies show that it should be possible to populate defect states near the vacuum level of alkalides with a laser pulse to produce long-lived defect electrons. Such preirradiated samples may then eject electrons thermionically at low temperatures or by the absorption of infrared photons.

Acknowledgment. This research was supported, in part, by NSF Grant DMR90-24525 and by the MSU Center for Fundamental Materials Research.

References and Notes

(1) Matalon, S.; Golden, S.; Ottolenghi, M. *J. Phys. Chem.* **1969**, *73*, 3098−3101.
(2) Dye, J. L.; DeBacker, M. G.; Nicely, V. A. *J. Am. Chem. Soc.* **1970**, *92*, 5226−5228.
(3) Dye, J. L.; Lok, M. T.; Tehan, F. J.; Coolen, R. B.; Papadakis, N.; Ceraso, J. M.; DeBacker, M. G. *Ber. Bunsenges. Phys. Chem.* **1971**, *75*, 659−662.
(4) Lok, M. T.; Tehan, F. J.; Dye, J. L. *J. Phys. Chem.* **1972**, *76*, 2975−2981.
(5) Dye, J. L. In *Electrons in Fluids*; Jortner, J., Kestner, N. R., Eds.; Springer-Verlag: Berlin, 1973; pp 77−95.
(6) Dye, J. L.; Ceraso, J. M.; Lok, M. T.; Barnett, B. L.; Tehan, F. J. *J. Am. Chem. Soc.* **1974**, *96*, 608−609.
(7) Tehan, F. J.; Barnett, B. L.; Dye, J. L. *J. Am. Chem. Soc.* **1974**, *96*, 7203−7208.
(8) Dye, J. L.; DeBacker, M. G. *Annu. Rev. Phys. Chem.* **1987**, *38*, 271−301.
(9) Dye, J. L. In *J. Phys. IV Colloque C5, Metals in Solution*; Damay, P., Leclerq, F., Eds.; les Éditions de Physique: Paris, 1991; Vol. 1, pp 259−282.
(10) Wagner, M. J.; Dye, J. L. *Annu. Rev. Mater. Sci.* **1993**, *23*, 223−253.
(11) Hendrickson, J. E. Ph.D. Thesis, Michigan State University, 1994.
(12) Dye, J. L.; Yemen, M. R.; DaGue, M. G.; Lehn, J.-M. *J. Chem. Phys.* **1978**, *68*, 1665−1670.
(13) Papaioannou, J.; Jaenicke, S.; Dye, J. L. *J. Solid State Chem.* **1987**, *67*, 122−130.
(14) Jaenicke, S.; Dye, J. L. *J. Solid State Chem.* **1984**, *54*, 320−329.
(15) Bannwart, R. S.; Solin, S. A.; DeBacker, M. G.; Dye, J. L. *J. Am. Chem. Soc.* **1989**, *111*, 5552−5556.
(16) Park, T.; Solin, S. A.; Dye, J. L. *Solid State Commun.* **1992**, *81*, 59−63.
(17) Park, T.; Solin, S. A.; Dye, J. L. *Phys. Rev. B.* **1992**, *46(II)*, 817−830.
(18) Xu, G.; Park, T.-R.; Bannwart, R. S.; Sieradzan, A.; DeBacker, M. G.; Solin, S. A.; Dye, J. L. In *Metals in Solution, J. Phys. IV-Colloque C5*; Damay, P., Leclerq, F., Eds.; les Éditions de Physique: Paris, 1991; Vol. 1; pp 283−290.
(19) Xu, G. Ph.D. Thesis, Michigan State University, 1992.
(20) Glarum, S. H.; Marshall, J. H. *J. Chem. Phys.* **1970**, *52*, 5555−5565.
(21) Huppert, D.; Bar-Eli, K. H. *J. Phys. Chem.* **1970**, *74*, 3285−3290.
(22) Friedenberg, A.; Levanon, H. *J. Phys. Chem.* **1977**, *81*, 766−771.
(23) DeBacker, M. G.; Sauvage, F. X.; Dye, J. L. *Chem. Phys. Lett.* **1990**, *73*, 291−297.
(24) Debacker, M. G.; Lacarriere, J. F.; Sauvage, F. X. In *J. Phys. IV, Metals in Solution, Colloque C5*; Damay, P., Leclerq, F., Eds.; les Éditions de Physique: Paris, 1991; Vol. 1; pp 297−301.
(25) Nelss, M. A.; Willard, J. E. *J. Phys. Chem.* **1975**, *79*, 783−794.
(26) Taft, E. A.; Philipp, H. R. *J. Phys. Chem. Solids* **1957**, *3*, 1−5.
(27) Kevan, L. In *Advances in Radiation Chemistry*; Burton, M., Magee, J. L., Eds.; Wiley-Interscience: New York, 1974; pp 275−298.
(28) Hager, S. L.; Willard, J. E. *J. Chem. Phys.* **1974**, *61*, 3244−3246.
(29) Klassen, N. V.; Gillis, H. A.; Walker, D. C. *J. Chem. Phys.* **1971**, *55*, 1979−1980.
(30) Klassen, N. V.; Gillis, H. A.; Teather, G. G. *J. Phys. Chem.* **1972**, *76*, 3847−3850.
(31) Klassen, N. V.; Gillis, H. A.; Teather, G. G. *J. Chem. Phys.* **1975**, *62*, 2474−2476.
(32) Issa, D.; Ellaboudy, A.; Janakiraman, R.; Dye, J. L. *J. Phys. Chem.* **1984**, *88*, 3847−3851.
(33) Shin, D.-H.; Ellaboudy, A. S.; Dye, J. L.; DeBacker, M. G. *J. Phys. Chem.* **1991**, *95*, 7085−7089.
(34) Shin, D. H. Ph.D. Thesis, Michigan State University, 1992.
(35) Shin, D.-H.; Dye, J. L.; Budil, D. E.; Earle, K. A.; Freed, J. H. *J. Phys. Chem.* **1993**, *97*, 1213−1219.
(36) Dye, J. L.; Andrews, C. W.; Mathews, S. E. *J. Phys. Chem.* **1975**, *79*, 3065−3070.
(37) VanEck, B.; Le, L. D.; Issa, D.; Dye, J. L. *Inorg. Chem.* **1982**, *21*, 1966−1970.
(38) Dye, J. L. *J. Phys. Chem.* **1980**, *84*, 1084−1090.
(39) Dye, J. L. *J. Phys. Chem.* **1984**, *88*, 3842−3846.
(40) Dye, J. L. *Chemtracts—Inorg. Chem.* **1993**, *5*, 243−270.
(41) Kuo, C.-T.; Dye, J. L.; Pratt, W. P., Jr., unpublished results, this laboratory, 1994.
(42) Huang, R. H.; Dye, J. L. *Chem. Phys. Lett.* **1990**, *166*, 133−136.
(43) Kane, E. O. *Phys. Rev.* **1962**, *127*, 131−141.

JP942314C

Global Tricompartmental Analysis of the Fluorescence Decay Surface of the Charged Fluorescent Probe *N,N,N*-Trimethyl-3-(1-pyrenyl)-1-propanaminium Perchlorate

Bart Hermans,[†] Frans C. De Schryver,*[,†] Noël Boens,[†] Marcel Ameloot,[‡] Robert Jérôme,[§] Phillippe Teyssié,[§] Erik Goethals,[∥] and Etienne Schacht[∥]

Department of Chemistry, Katholieke Universiteit Leuven, B-3001 Heverlee-Leuven, Belgium, Limburgs Universitair Centrum, B-3590 Diepenbeek, Belgium, Université de Liège, Sart Tilman B-4000 Liège, Belgium, and Rijksuniversteitit Gent, B-9000 Gent, Belgium

Received: September 26, 1994[⊗]

The kinetics of the excited-state processes of the charged fluorescent probe *N,N,N*-trimethyl-3-(1-pyrenyl)-1-propanaminium perchlorate (PROBE) in tetrahydrofuran are reported. At very low concentrations PROBE decays monoexponentially with a lifetime τ of 236 ± 1 ns, from which $k_{01} = 1/\tau = 4.2 \times 10^6\ s^{-1}$ is obtained. Upon addition of the quaternary ammonium salt *N,N,N*-trimethyl-1-dodecanaminium perchlorate a biexponential decay function is needed to describe the decay traces. The second excited state is the aggregated PROBE. This aggregation is due to dipole−dipole or ion−dipole interactions. The rate constant values of the kinetic Scheme (Scheme 4) are obtained by global bicompartmental analysis: $k_{01} = k_{02}$, $k_{21} = (42 \pm 7) \times 10^9\ M^{-1}\ s^{-1}$; $k_{12} = (5.7 \pm 0.1) \times 10^7\ s^{-1}$. When the concentration of PROBE itself is varied, a triple-exponential decay function adequately describes the decay surface. The third excited-state species is a PROBE excimer, which can be formed through two different pathways: either intermolecularly when a locally excited PROBE molecule encounters a ground-state PROBE molecule or intramolecularly when an aggregate of two PROBE molecules rearranges. To resolve the kinetics of this system, global tricompartmental analysis is developed. Even after including the information available from experiments where *N,N,N*-trimethyl-1-dodecanaminium perchlorate is added ($k_{01} = k_{02}$), and the information available from the global triple-exponential analysis ($k_{13} = 0$ and $k_{23} = 0$) (Scheme 5), the experimental time-resolved data do not allow one to obtain a unique solution for the rate constant values. By scanning the rate constant k_{31}, bounds can be specified for the rate constants: $53 \times 10^9 < k_{21} < 60 \times 10^9\ M^{-1}\ s^{-1}$, $k_{31} < 7 \times 10^9\ M^{-1}\ s^{-1}$, $1.5 \times 10^8 < k_{12} < 1.7 \times 10^8\ s^{-1}$, and $k_{32} < 2 \times 10^7\ s^{-1}$. Unique values are obtained for k_{01}, k_{02}, and k_{03}: $k_{01} = k_{02} = (4.25 \pm 0.01) \times 10^7\ s^{-1}$; $k_{03} = (1.92 \pm 0.03) \times 10^7\ s^{-1}$.

1. Introduction

The introduction of ionic units into neutral polymers drastically changes the properties of these materials. In polar solvents the counterions can be readily solvated, resulting in a polymer backbone that covalently links several free charges. The behavior of these charged macromolecules in polar solvents is known in the literature as the polyelectrolyte behavior.[1] In less polar solvents ($\epsilon < 15$) the counterions will stay closer to the ionic units on the chain. Contact ion pairs and solvent-separated ion pairs are more likely to be formed than free ions. These contact ion pairs can be regarded as dipoles, and ion−dipole and dipole−dipole interactions occur in these media.[2] In the literature this behavior is referred to as the ion aggregate behavior.[3−17]

Since the intra- and interchain interactions seem to be important in the model describing the ion aggregate behavior, it can be expected that intra- and intermolecular excimer formation is an excellent tool to obtain information about the ion aggregation. Stationary fluorescence measurements of a fluorescent probe attached to both ends of a polystyrene−halato telechelic polymer (HTP)—have been used to discriminate between intra- and interchain associations.[18] It was shown that at low concentrations the intrachain dipole−dipole interactions prevail and that upon increasing the concentration, the interchain interactions start to dominate.

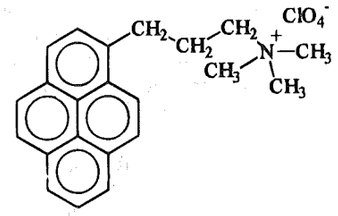

Figure 1. *N,N,N*-Trimethyl-3-(1-pyrenyl)-1-propanaminium perchlorate.

Up to now, no kinetic information was available on the ion aggregation behavior. Time-resolved emission spectroscopy can provide detailed kinetic information about this phenomenon for fluorescently labeled HTP. To understand the information obtained by a reporter fluorophore-capped polymer backbone, the kinetic behavior of the probe itself must be elucidated first. Therefore, the charged fluorescence probe *N,N,N*-trimethyl-3-(1-pyrenyl)-1-propanaminium perchlorate, PROBE (Figure 1), was synthesized.

In this paper the kinetics of the excited-state processes of PROBE in tetrahydrofuran are reported. The experimental fluorescence decay traces are analyzed simultaneously to enhance the capacity to distinguish between competing models and to obtain the most reliable parameter estimates. By use of the global compartmental analysis,[19] an extension of the global analysis approach,[20−22] values of the rate constants, the normalized ground-state absorbances, and the normalized emission

* To whom correspondence should be addressed.
[†] Katholieke Universiteit Leuven.
[‡] Limburgs Universitair Centrum.
[§] Université de Liège.
[∥] Rijksuniverstiteit Gent.
[⊗] Abstract published in *Advance ACS Abstracts,* November 15, 1994.

0022-3654/94/2098-13583$04.50/0

SCHEME 1

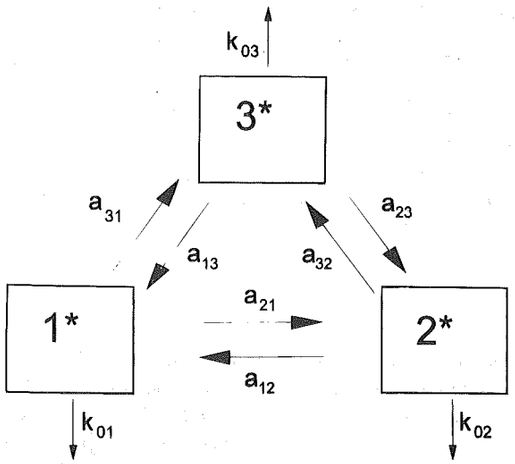

SCHEME 2

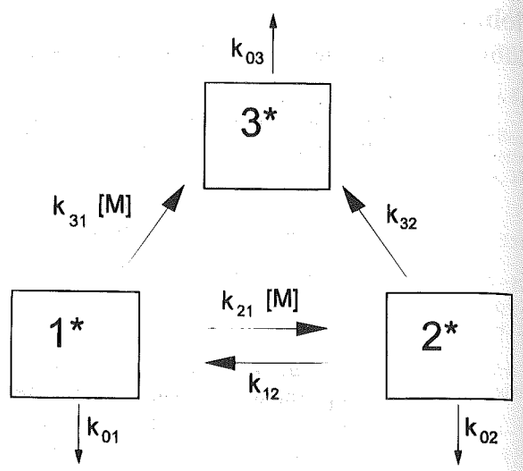

weighting factors can be determined. The global compartmental analysis approach is the method of choice to unravel very complex kinetics, as is the case here.

2. Theory

2.1. Kinetics. Consider a causal, linear, time-invariant, photophysical system consisting of three distinct ground-state species (1, 2, 3) and three corresponding excited-state species (1*, 2*, 3*), as depicted in Scheme 1. The excited-state species can decay by fluorescence (F) and nonradiative processes (NR) (internal conversion (IC) and intersystem crossing (ISC)). The composite rate constants for these processes are denoted by k_{01} ($=k_{F1} + k_{IC1} + k_{ISC1}$), k_{02} ($=k_{F2} + k_{IC2} + k_{ISC2}$), and k_{03} ($=k_{F3} + k_{IC3} + k_{ISC3}$). The interconversion $j^* \rightarrow i^*$ is described by a_{ij}. The transformation can be either monomolecular ($a_{ij} = k_{ij}$) or bimolecular ($a_{ij} = k_{ij}$ [M]) where k_{ij} denotes the rate constant for the interconversion and [M] is the concentration.

After excitation, which does not significantly alter the concentrations of the ground-state species, the fluorescence δ-response function, $f(\lambda^{em},\lambda^{ex},t)$, at emission wavelength λ^{em} due to excitation at λ^{ex} is expressed by[19]

$$f(\lambda^{em},\lambda^{ex},t) = \mathbf{c}(\lambda^{em})\mathbf{U}\exp(t\Gamma)\mathbf{U}^{-1}\mathbf{b}(\lambda^{ex}) \qquad t \geq 0 \quad (1)$$

$\mathbf{U} \equiv [\mathbf{U_1},\mathbf{U_2},\mathbf{U_3}]$ is the matrix of the three eigenvectors of matrix $\mathbf{A}$ (eq 2) and $\mathbf{U}^{-1}$ the inverse of $\mathbf{U}$. γ_1, γ_2, and γ_3 are the eigenvalues of $\mathbf{A}$ corresponding to $\mathbf{U_1}$, $\mathbf{U_2}$, and $\mathbf{U_3}$, and $\exp(t\Gamma) \equiv \mathrm{diag}\{\exp(\gamma_1 t), \exp(\gamma_2 t), \exp(\gamma_3 t)\}$.

$$A = \begin{bmatrix} -(k_{01} + a_{21} + a_{31}) & a_{12} & a_{13} \\ a_{21} & -(k_{02} + a_{12} + a_{32}) & a_{23} \\ a_{31} & a_{32} & -(k_{03} + a_{13} + a_{23}) \end{bmatrix} \quad (2)$$

$\mathbf{b}(\lambda^{ex})$ is the 3×1 vector of the excited-state concentrations at time zero,

$$b = \begin{bmatrix} b_1 \\ b_2 \\ b_3 \end{bmatrix} = \begin{bmatrix} [1^*](0) \\ [2^*](0) \\ [3^*](0) \end{bmatrix} \quad (3)$$

$\mathbf{b}$ is dependent on the excitation wavelength λ^{ex} and on [M]. $\mathbf{c}(\lambda^{em})$ is the 1×3 vector of the spectral emission weighting factors $c_i(\lambda^{em})$ of species i^* at emission wavelength λ^{em}.[19] $\mathbf{c}$ is dependent on the emission wavelength only.

Defining the normalized elements $\tilde{b}_i$ and $\tilde{c}_i$,

$$\tilde{b}_i = b_i/(b_1 + b_2 + b_3) \quad \text{for} \quad i = 1, 2, 3 \quad (4)$$

$$\tilde{c}_i = c_i/(c_1 + c_2 + c_3) \quad \text{for} \quad i = 1, 2, 3 \quad (5)$$

Equation 1 can be written as

$$f(\lambda^{em},\lambda^{ex},t) = \kappa\tilde{\mathbf{c}}(\lambda^{em})\mathbf{U}\exp(t\Gamma)\mathbf{U}^{-1}\tilde{\mathbf{b}}(\lambda^{ex}) \qquad t \geq 0 \quad (6)$$

with κ a proportionality constant.

Assuming (i) that the interconversions $1^* \rightarrow 2^*$ and $1^* \rightarrow 3^*$ are bimolecular and therefore have to be described by the second-order rate constants k_{21} and k_{31}, respectively, (ii) that the processes $2^* \rightarrow 1^*$ and $2^* \rightarrow 3^*$ are monomolecular and are specified by the first-order rate constants k_{12} and k_{32}, respectively, and (iii) that the interconversions $3^* \rightarrow 1^*$ and $3^* \rightarrow 2^*$ are negligibly slow, Scheme 1 simplifies to Scheme 2. This scheme describes the kinetic behavior of PROBE in tetrahydrofuran, as will be evident from the analysis.

In this case matrix $\mathbf{A}$ (eq 2) can be simplified to

$$A = \begin{bmatrix} -k_{01} - k_{21}[M] - k_{31}[M] & k_{12} & 0 \\ k_{21}[M] & -k_{02} - k_{12} - k_{32} & 0 \\ k_{31}[M] & k_{32} & -k_{03} \end{bmatrix} \quad (7)$$

The exponential factors γ_i are related to the decay times

$$\gamma_i = -1/\tau_i \quad (8)$$

and are explicitly given by

$$\gamma_1 = -k_{03} \quad (9)$$

$$\gamma_2 = -(1/2)\{(S_1 + S_2) - [(S_1 - S_2)^2 + 4P[M]]^{1/2}\} \quad (10)$$

$$\gamma_3 = -(1/2)\{(S_1 + S_2) + [(S_1 - S_2)^2 + 4P[M]]^{1/2}\} \quad (11)$$

with

$$S_1 = k_{01} + (k_{21} + k_{31})[M] \quad (12)$$

$$S_2 = k_{02} + k_{12} + k_{32} \quad (13)$$

$$P = k_{12}k_{21} \quad (14)$$

From eqs 9−11 it is clear that only one decay time (see eq 9) relates directly to a specific excited-state species. γ_2 and γ_3 are functions of k_{ij} and [M] and can, therefore, not be related to a particular excited state. The concentration dependence of γ_2 and γ_3 allows one to obtain information on the rate constants. Plots of the corresponding decay times as a function of [M] indicate the concentration ranges required to obtain this information. The decay time corresponding to γ_1 ($\tau_1 = -1/k_{03}$) is independent of [M]. At low concentrations one other decay time will equal the value of $1/k_{01}$ and the last one equals the value of $1/(k_{02} + k_{12} + k_{32})$. At high concentrations the limiting values are 0 and $1/(k_{02} + k_{12}\,k_{31}/(k_{21} + k_{31}) + k_{32})$. The concentration range where the decay times vary are mainly determined by k_{21} and k_{31}. Depending on the relation between the values of k_{01} and $(k_{02} + k_{12} + k_{32})$, two types of concentration-dependent behavior can be found. Each of these types can be subdivided into three classes according to the relative value of k_{03}.

Type A: $k_{01} > (k_{02} + k_{12} + k_{32})$. Besides the concentration-independent decay time, there are two additional decay times: a shorter (τ_S) and a longer (τ_L) one. τ_L increases while τ_S decreases upon increasing the concentration of M. At very low concentrations τ_S equals $1/k_{01}$, whereas τ_L equals $1/(k_{02} + k_{12} + k_{32})$. Upon increasing [M], τ_S decreases and has a zero limiting value. τ_L, on the contrary, increases to finally reach the limiting value of $1/(k_{02} + k_{12}k_{31}/(k_{21} + k_{31}) + k_{32})$. It can readily be shown that, if k_{21} is negligible compared to k_{31}, the limiting value for τ_L at high [M] is $1/(k_{02} + k_{12} + k_{32})$. Then τ_L is virtually independent of the concentration. If $k_{12} = 0$, τ_L remains constant at $1/(k_{02} + k_{32})$ as a function of [M].

Class 1: $k_{03} > k_{01} > (k_{02} + k_{12} + k_{32})$. For this class the constant decay time crosses τ_S (see Figure 2a). If $k_{12} = 0$ or $k_{21} \ll k_{31}$, then two decay times remain constant. The variable decay time is crossed by one constant decay time (see Figure 3a).

Class 2: $k_{01} > k_{03} > (k_{02} + k_{12} + k_{32})$. In this case the constant decay time always lies between τ_S and τ_L (see Figure 2b). If $k_{12} = 0$ or $k_{21} \ll k_{31}$, then two decay times remain constant. The variable decay time always lies under the two constant decay times (see Figure 3b).

Class 3: $k_{01} > (k_{02} + k_{12} + k_{32}) > k_{03}$. For this class the constant decay time lies above both other decay times (see Figure 2c). If $k_{12} = 0$ or $k_{21} \ll k_{31}$, then the situation is similar to that in Figure 3b (see Figure 3c).

From Figure 3a−c it is evident that when $k_{12} = 0$ or $k_{21} \ll k_{31}$, only a value for k_{01} can be assigned corresponding to the variable decay time at low [M]. Such systems are unidentifiable.

Type B: $(k_{02} + k_{12} + k_{32}) > k_{01}$. Besides the concentration-independent decay time, there are two additional decay times, which both decrease upon increasing [M]. At very low [M] τ_S equals $1/(k_{02} + k_{12} + k_{32})$, whereas τ_L equals $1/k_{01}$. Upon increasing the concentration of [M], τ_S decreases and goes to 0. If $(k_{02} + k_{12}k_{31}/(k_{21} + k_{31}) + k_{32}) < k_{01}$, τ_L increases and reaches the limiting value of $1/(k_{02} + k_{12}k_{31}/(k_{21} + k_{31}) + k_{32})$. In this case the concentration dependence of τ_i is similar to type A behavior (see Figures 2 and 3). If, however, $(k_{02} + k_{12}k_{31}/(k_{21} + k_{31}) + k_{32}) > k_{01}$, τ_L decreases to the same limiting value. Only this case will be discussed below. Two decay times which decrease with increasing [M] is compatible only with type B. If k_{21} is negligible compared to k_{31}, the limiting value for τ_L at high [M] is $1/(k_{02} + k_{12} + k_{32})$. If $k_{12} = 0$, the limiting value for τ_L at high [M] is equal to the limiting value for τ_S at low [M] and equals $1/(k_{02} + k_{32})$. In both cases it might look as if a constant decay time crosses the variable one.

Class 1: $k_{03} > (k_{02} + k_{12} + k_{32}) > k_{01}$. In this case, the constant decay time crosses τ_S (see Figure 4a). If $k_{12} = 0$ or $k_{21} \ll k_{31}$, then it looks as if two decay times are independent of [M] and cross the variable decay time.

Class 2: $(k_{02} + k_{12} + k_{32}) > k_{03} > k_{01}$. For this class, the constant decay time crosses τ_L(see Figure 4b). If $k_{12} = 0$ or $k_{21} \ll k_{31}$, then it looks as if two decay times remain constant and cross the variable decay time.

Class 3: $(k_{02} + k_{12} + k_{32}) > k_{01} > k_{03}$. In this case the constant decay time is always the longest one (see Figure 4c). If $k_{12} = 0$ or $k_{21} \ll k_{31}$, then it looks as if the variable decay time is crossed by the lowest constant decay time. This situation looks similar to that of type A class 1 (see Figure 3a).

When $k_{12} = 0$ or $k_{21} \ll k_{31}$, experimentally only one concentration-dependent decay time will be observed. A value for k_{01} can be assigned corresponding to this variable decay time at low [M]. Such systems are unidentifiable. Note that this was also the case for type A systems.

2.2. Identifiability. In the identifiability study we shall examine if the rate constants k_{ij} can be uniquely determined

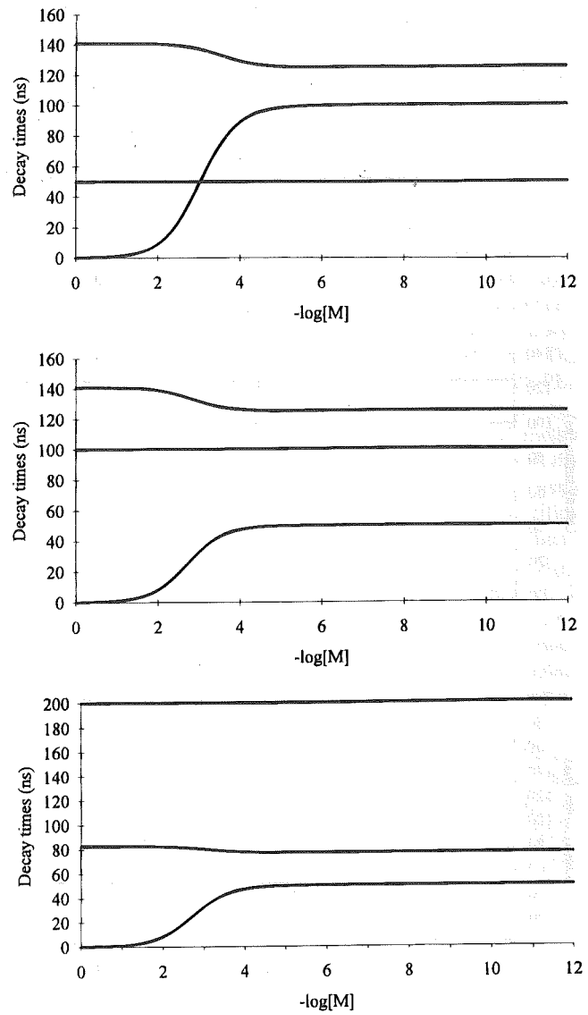

Figure 2. (a, top) Decay times (eqs 8−11) as a function of −log [M] calculated with $k_{01} = 0.01 \times 10^9$ s^{-1}, $k_{21} = 9 \times 10^9$ M^{-1} s^{-1}, $k_{31} = 1 \times 10^9$ M^{-1} s^{-1}, $k_{02} = 0.005 \times 10^9$ s^{-1}, $k_{12} = 0.001 \times 10^9$ s^{-1}, $k_{32} = 0.002 \times 10^9$ s^{-1}, and $k_{03} = 0.02 \times 10^9$ s^{-1}. (b, middle) Decay times (eqs 8−11) as a function of −log [M] calculated with $k_{01} = 0.02 \times 10^9$ s^{-1}, $k_{21} = 9 \times 10^9$ M^{-1} s^{-1}, $k_{31} = 1 \times 10^9$ M^{-1} s^{-1}, $k_{02} = 0.005 \times 10^9$ s^{-1}, $k_{12} = 0.001 \times 10^9$ s^{-1}, $k_{32} = 0.002 \times 10^9$ s^{-1}, and $k_{03} = 0.01 \times 10^9$ s^{-1}. (c, bottom) Decay times (eqs 8−11) as a function of −log [M] calculated with $k_{01} = 0.02 \times 10^9$ s^{-1}, $k_{21} = 9 \times 10^9$ M^{-1} s^{-1}, $k_{31} = 1 \times 10^9$ M^{-1} s^{-1}, $k_{02} = 0.01 \times 10^9$ s^{-1}, $k_{12} = 0.001 \times 10^9$ s^{-1}, $k_{32} = 0.002 \times 10^9$ s^{-1}, $k_{03} = 0.005 \times 10^9$ s^{-1}.

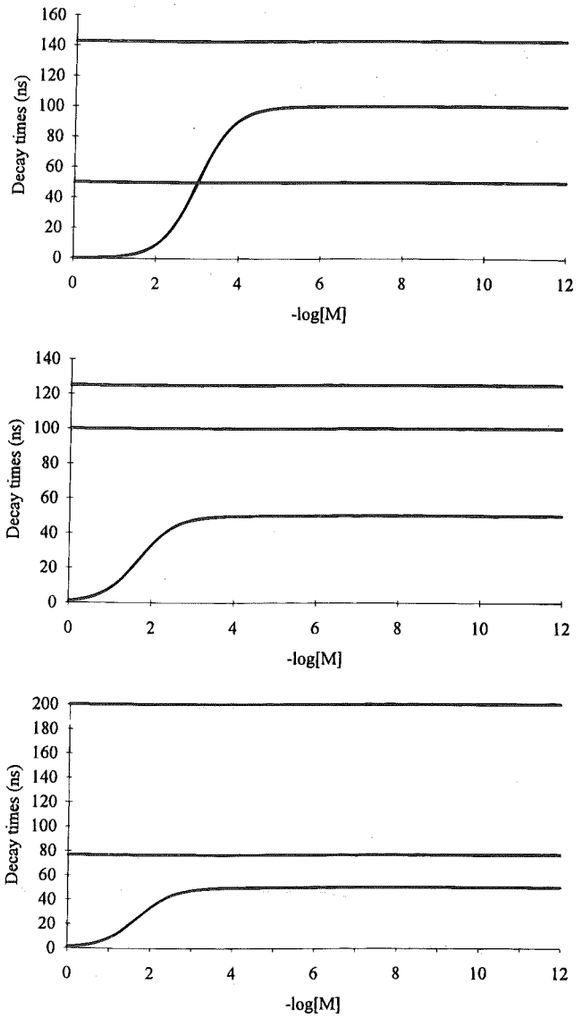

Figure 3. (a, top) Decay times (eqs 8−11) as a function of −log [M] calculated with $k_{01} = 0.01 \times 10^9\ s^{-1}$, $k_{21} = 9 \times 10^9\ M^{-1}\ s^{-1}$, $k_{31} = 1 \times 10^9\ M^{-1}\ s^{-1}$, $k_{02} = 0.005 \times 10^9\ s^{-1}$, $k_{12} = 0\ s^{-1}$, $k_{32} = 0.002 \times 10^9\ s^{-1}$, and $k_{03} = 0.02 \times 10^9\ s^{-1}$. (b, middle) Decay times (eqs 8−11) as a function of −log [M] calculated with $k_{01} = 0.02 \times 10^9\ s^{-1}$, $k_{21} = 1 \times 10^5\ M^{-1}\ s^{-1}$, $k_{31} = 1 \times 10^9\ M^{-1}\ s^{-1}$, $k_{02} = 0.005 \times 10^9\ s^{-1}$, $k_{12} = 0.001 \times 10^9\ s^{-1}$, $k_{32} = 0.002 \times 10^9\ s^{-1}$, and $k_{03} = 0.01 \times 10^9\ s^{-1}$. (c, bottom) Decay times (eqs 8−11) as a function of −log [M] calculated with $k_{01} = 0.02 \times 10^9\ s^{-1}$, $k_{21} = 1 \times 10^5\ M^{-1}\ s^{-1}$, $k_{31} = 1 \times 10^9\ M^{-1}\ s^{-1}$, $k_{02} = 0.01 \times 10^9\ s^{-1}$, $k_{12} = 0.001 \times 10^9\ s^{-1}$, $k_{32} = 0.002 \times 10^9\ s^{-1}$, and $k_{03} = 0.005 \times 10^9\ s^{-1}$.

under error free conditions. Consider the specific case depicted by Scheme 2 with the system matrix **A** given by eq 7, for which the following functions can be defined for a given probe concentration $[M]_k$.

$$\sigma_{1,k} = \gamma_1 + \gamma_2 + \gamma_3 = -B - A[M]_k \tag{15}$$

with

$$A = k_{21} + k_{31} \tag{16}$$

$$B = k_{01} + k_{02} + k_{12} + k_{32} + k_{03} \tag{17}$$

$$\sigma_{2,k} = \gamma_1\gamma_2 + \gamma_1\gamma_3 + \gamma_2\gamma_3 = D + C[M]_k \tag{18}$$

with

$$C = k_{21}(k_{02} + k_{03} + k_{32}) + k_{31}(k_{02} + k_{12} + k_{32} + k_{03}) \tag{19}$$

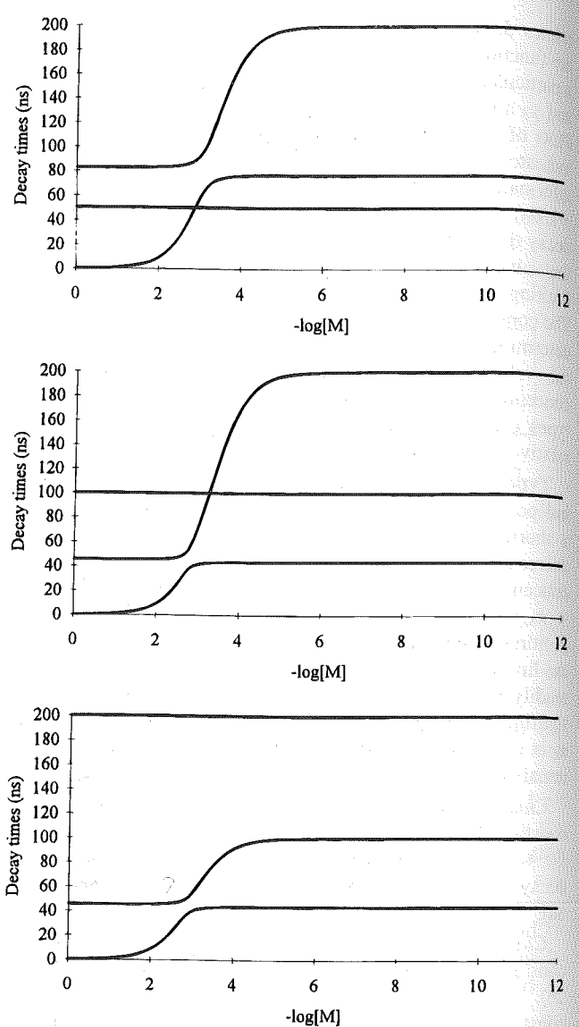

Figure 4. (a, top) Decay times (eqs 8−11) as a function of −log [M] calculated with $k_{01} = 0.005 \times 10^9\ s^{-1}$, $k_{21} = 9 \times 10^9\ M^{-1}\ s^{-1}$, $k_{31} = 1 \times 10^9\ M^{-1}\ s^{-1}$, $k_{02} = 0.01 \times 10^9\ s^{-1}$, $k_{12} = 0.001 \times 10^9\ s^{-1}$, $k_{32} = 0.002 \times 10^9\ s^{-1}$, and $k_{03} = 0.02 \times 10^9\ s^{-1}$. (b, middle) Decay times (eqs 8−11) as a function of −log [M] calculated with $k_{01} = 0.005 \times 10^9\ s^{-1}$, $k_{21} = 9 \times 10^9\ M^{-1}\ s^{-1}$, $k_{31} = 1 \times 10^9\ M^{-1}\ s^{-1}$, $k_{02} = 0.02 \times 10^9\ s^{-1}$, $k_{12} = 0.001 \times 10^9\ s^{-1}$, $k_{32} = 0.002 \times 10^9\ s^{-1}$, and $k_{03} = 0.01 \times 10^9\ s^{-1}$. (c, bottom) Decay times (eqs 8−11) as a function of −log [M] calculated with $k_{01} = 0.01 \times 10^9\ s^{-1}$, $k_{21} = 9 \times 10^9\ M^{-1}\ s^{-1}$, $k_{31} = 1 \times 10^9\ M^{-1}\ s^{-1}$, $k_{02} = 0.02 \times 10^9\ s^{-1}$, $k_{12} = 0.001 \times 10^9\ s^{-1}$, $k_{32} = 0.002 \times 10^9\ s^{-1}$, and $k_{03} = 0.005 \times 10^9\ s^{-1}$.

$$D = k_{01}(k_{02} + k_{12} + k_{32}) + k_{03}(k_{02} + k_{12} + k_{32}) + k_{01}k_{03} \tag{20}$$

$$\sigma_{3,k} = \gamma_1\gamma_2\gamma_3 = -F - E[M]_k \tag{21}$$

with

$$E = k_{03}[k_{21}(k_{02} + k_{32}) + k_{31}(k_{02} + k_{12} + k_{32})] \tag{22}$$

$$F = k_{01}k_{03}(k_{02} + k_{12} + k_{32}) \tag{23}$$

Considering two different concentrations of the probe, $[M]_k$ and $[M]_l$, where the decay times vary, the expressions A through F can be evaluated, which will be used to obtain information on the rate constants.

Equations 17, 20, and 23 can be combined to yield

$$k_{03}^3 - k_{03}^2 B + k_{03} D - F = 0 \tag{24}$$

The combination of eqs 16, 19, and 22 gives

$$k_{03}^2 - C/A k_{03} + E/A = 0 \tag{25}$$

Since eqs 24 and 25 do not divide, the common root of both equations allows one to assign a unique value to k_{03}.

Analogously, for k_{01} and $(k_{02} + k_{12} + k_{32})$, from eqs 17, 20, and 23 we have

$$k_{01}^3 - k_{01}^2 B + k_{01} D - F = 0 \tag{26}$$

$$(k_{02} + k_{12} + k_{32})^3 - (k_{02} + k_{12} + k_{32})^2 B + (k_{02} + k_{12} + k_{32}) D - F = 0 \tag{27}$$

Solution of eqs 24, 26, and 27 yields three roots, one of which can be uniquely assigned to k_{03}. However we are not able to univocally assign the other values to k_{01} and $(k_{02} + k_{12} + k_{32})$ without additional information. The concentration dependence (Figures 2−4) may provide the lacking information. If the two variable decay times decrease with increasing [M], which can only be the case for type B, we have that $(k_{02} + k_{12} + k_{32}) > k_{01}$. This automatically establishes the proper assignment. If one decay time increases, the assignment cannot be made and two sets of solutions are mathematically possible. However, at $[M] = 0$ the monoexponential decay yields the unique value for k_{01}.

Once a value for k_{01} is assigned and the value for k_{02} is known, bounds on the rate constants (k_{21}, k_{31}, k_{12}, k_{32}) can be specified as follows. Equation 17 yields a value for B^*:

$$B^* = B - k_{01} - k_{02} - k_{03} = k_{12} + k_{32} \tag{28}$$

Combining eqs 16, 17, and 19 yields

$$C^* = A(B - k_{01}) - C = k_{12}k_{21} \tag{29}$$

Equations 16, 28, and 29 provide the basis for the determination of the interconversion rate constants (k_{21}, k_{31}, k_{12}, k_{32}). Thus, only three independent equations are available to determine four unknown rate constant values. Therefore, a unique set of values for those rate constants cannot be obtained. It is, however, possible to obtain information from these data. For each value assigned to one of the rate constants k_{21}, k_{31}, k_{12}, and k_{32}, the corresponding values of the remaining rate constants can be determined within the following limits:[23]

$$0 < k_{31} < A - C^*/B^* \tag{30}$$

$$C^*/B^* < k_{21} < A \tag{31}$$

$$0 < k_{32} < B^* - C^*/A \tag{32}$$

$$C^*/A < k_{12} < B^* \tag{33}$$

3. Experimental Section

3.1. Materials. l-Pyrenecarbaldehyde, (carbethoxymethylene)triphenylphosphorane, toluene (99%), Pd/C, $LiAlH_4$, PBr_3, dichloromethane (>99%), and *tert*-butyl methyl ether were purchased from Janssen (Geel, Belgium). Ethanol (>99%) and the ion exchanger (stark basischer Anionenaustauscher) were obtained from Merck (Darmstadt, Germany). Tetrahydrofuran (THF, HPLC) was supplied by Rathburn (Walkerburn, Scotland), and trimethylamine by UCAR (Olen, Belgium). Methanol (HPLC), hexane (HPLC), dichlormethane (HPLC), tetra-*tert*-butyl-ammonium perchlorate (t-BUTAP), and *N,N,N*-trimethyl-1-dodecanaminium perchlorate (DOTAP) were obtained from Fluka (Buchs, Switzerland). The thin layer silica gel plates (DC Fertigplatten SIL G-200) were purchased from Macherey-Nagel (Düren, Germany). Quinine sulfate and HClO4 were from Aldrich (Bornem, Belgium), and 0.1 N sulfuric acid from Riedel-de Haën (Seelze, Germany). The solvents were used as received unless otherwise specified.

3.2. Synthesis of PROBE. l-Pyrenecarbaldehyde is modified in a Wittig reaction using (carbethoxymethylene)triphenylphosphorane in toluene to afford ethyl 3-(1-pyrenyl)-2-propenoate. This compound is reduced to ethyl 3-(1-pyrenyl)-propanoate under hydrogen pressure in a 1:1 ethanol/THF mixture in the presence of Pd/C catalyst. Further reduction with LiAlH4 in dry THF yields 3-(1-pyrenyl)-1-propanol. This alcohol is converted into the corresponding bromide with PBr_3 in a 1:1 toluene/dichloromethane mixture. The quaternary ammonium salt with bromide counterion in *tert*-butyl methyl ether is produced upon bubbling with trimethylamine. PROBE is obtained by an ion exchange (Br^- exchanged for OH^-) using water as solvent, followed by a titration with $HClO_4$. Identification of the final product by ^1H NMR: (δ; multiplicity; integration; origin); (2.4; multiplet; 2; $PyCH_2CH_2CH_2N^+(CH_3)_3$); (3.2; singlet; 9; $PyCH_2CH_2CH_2N^+(CH_3)_3$); (3.4; triplet; 2; $PyCH_2CH_2CH_2N^+(CH_3)_3$); (3.6; triplet; 2; $PyCH_2CH_2CH_2N^+(CH_3)_3$); (8.2; multiplet; 9; $PyCH_2CH_2CH_2N^+(CH_3)_3$). Elemental analysis confirmed that the ion exchange was complete: (element; theoretical value; experimental value); (Cl; 8.84; 8.26); (Br; 17.8−18.2; <0.1).

3.3. Sample Preparation. PROBE solutions were prepared in THF or methanol. t-BUTAP and DOTAP were used as added salts. Both products were recrystallized from ethanol. All solutions were degassed using five freeze−pump−thaw cycles. Before use 1-methylpyrene was purified by thin layer chromatography on silica gel with 50% dichloromethane in hexane. Most experiments were performed in THF because the aggregation phenomenon is to be expected in this solvent. As THF is known to be an associating solvent,[24] no corrections were made for the ionic strength.

3.4. Absorption and Stationary and Time-Resolved Fluorescence Measurements. Absorption spectra were recorded on a Perkin-Elmer Lambda 6 UV/vis spectrophotometer coupled to an IBM PS/2. Excitation spectra (emission wavelength: 378 nm) and the corrected steady-state fluorescence spectra (excitation wavelength: 344 nm) were recorded on an SLM Aminco 8000C spectrofluorimeter.

Fluorescence decay curves were obtained using a Spectra-Physics mode-locked, synchronously pumped, cavity-dumped, frequency-doubled DCM dye laser as excitation source (excitation wavelength: 320 nm) with single photon timing detection. A detailed description of the apparatus has been given elsewhere.[25] All decays had 1/2K data points with approximately 3×10^3 counts in the peak channel. All solutions where excimers are formed were measured in the front phase configuration using quartz cells with 1 mm path length. Low-concentration solutions were measured in the right angle configuration using quartz cells with 1 cm path length. The emission polarizer was set at the magic angle configuration. All measurements were performed at ambient temperature.

The fluorescence quantum yields of the probes were determined with quinine sulfate in 0.1 N sulfuric acid as a reference.[26] Correction for the refractive index was applied.

3.5. Data Analysis. The global compartmental analysis of the fluorescence decay surface of species undergoing excited-state processes was implemented in the existing general global analysis program[25] based on Marquardt's[27] algorithm.

Consider the excited-state processes depicted by Scheme 2.

The global fitting parameters are k_{ij}, $\tilde{b}_k$, and $\tilde{c}_k$ ($k = 1, 2$). The only local fitting parameters are the scaling factors. Using this approach, experiments done at different excitation/emission wavelengths and at multiple timing calibrations and PROBE and ammonium salt concentrations are linked by all rate constants defining the system.

The fitting parameters were determined by minimizing the global reduced χ_g^2:

$$\chi_g^2 = \sum_{l}^{q}\sum_{i} w_{li}(y_{li}^o - y_{li}^c)^2/\nu \qquad (34)$$

where the index l sums over q experiments, and the index i sums over the appropriate channel limits for each individual experiment. y_{li}^o and y_{li}^c denote respectively the observed (experimentally measured) and calculated (fitted) values corresponding to the ith channel of the lth experiment, and w_{li} is the corresponding statistical weight. ν represents the number of degrees of freedom for the entire multidimensional fluorescence decay surface.

The statistical criteria to judge the quality of the fit include both graphical and numerical tests. The graphical methods comprised plots of surfaces of the autocorrelation function values vs experiment number and of the weighted residuals vs channel number vs experiment number. The numerical statistical tests incorporated the calculation of χ_g^2 and its corresponding $Z_{\chi_g^2}$:

$$Z_{\chi_g^2} = (\nu/2)^{1/2}(\chi_g^2 - 1) \qquad (35)$$

The additional statistical criteria to judge the quality of the fit are described elsewhere.[28]

4. Results and Discussion

4.1. The Properties of PROBE at Very Low Concentration. Since PROBE covalently links a quaternary ammonium salt to a pyrene moiety, a 1:1 stoichiometry between the ammonium salt and the fluorophore is established irrespective of the concentration.

Several authors have mentioned interactions between aromatic chromophores and quaternary ammonium groups.[29,30] A close contact between the salt and the aromatic moiety, which can be established at the surface of a micelle or at very high concentrations in solution, is believed to be necessary to obtain quenching by the ammonium salt. The exact mechanism of this quenching process, however, has not been established.

To check whether there is an influence of the quaternary ammonium salt on the pyrene moiety in THF, spectroscopic measurements of PROBE were compared with those of 1-methylpyrene.

4.1.1. Stationary Measurements. The absorption spectrum of PROBE shows a small deviation, especially the ^1L_b band, compared to the absorption band of 1-methylpyrene (Figure 5). The fact that the ^1L_b rather than the ^1L_a band is influenced is also seen in the normalized emission spectra (Figure 6) and the normalized excitation spectra (Figure 7). The emission spectra show a shift in intensity demonstrating the influence from the ammonium group on the ^1L_b band. The excitation spectra, however, show no clear shift, suggesting that there is no influence on the ^1L_a band.

The fluorescence quantum yield of PROBE was determined to be 0.74 ± 0.07. For 1-methylpyrene a similar value of 0.71 $\pm$ 0.07 was found.

4.1.2. Time-Resolved Fluorescence Measurements. At very low concentrations (1×10^{-6} M) of PROBE the emission decays monoexponentially with a lifetime of 236 ± 1 ns, from which $k_{01} = k_F + k_{NR} = 4.2 \times 10^6$ s^{-1} can be calculated. An analogous solution of 1-methylpyrene has a lifetime of 191 ± 1 ns and a related rate constant $k_{01} = 5.2 \times 10^6$ s^{-1}.

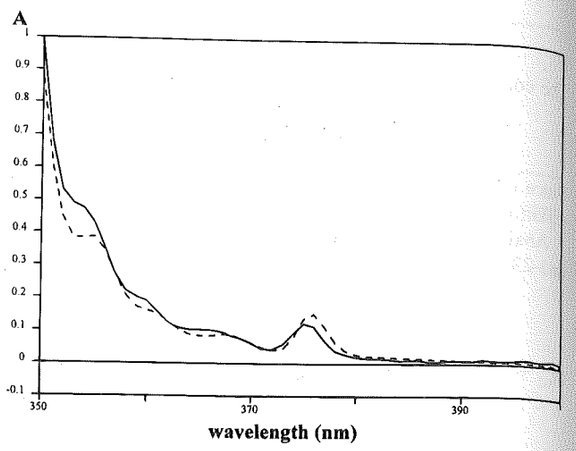

Figure 5. Absorption spectra of PROBE (dashed line) and 1-methylpyrene (full line) in THF.

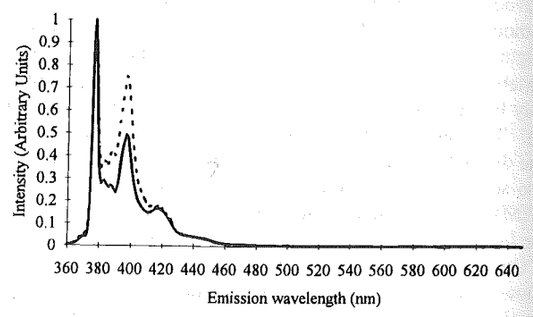

Figure 6. Emission spectra (normalized at 377 nm) of 1-methylpyrene (full line) and PROBE (dashed line) in THF.

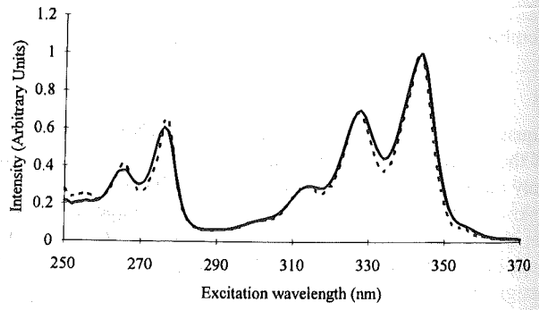

Figure 7. Excitation spectra (normalized at 343 nm) of 1-methylpyrene (full line) and PROBE (dashed line) in THF.

From the lifetime and fluorescence quantum yield the values for the radiative (k_F) and nonradiative (k_{NR}) rate constants can be calculated. For PROBE, values of $(3.1 \pm 0.3) \times 10^6$ s^{-1} for k_F and $(1.1 \pm 0.1) \times 10^6$ s^{-1} for k_{NR} were calculated. For 1-methylpyrene a value if $(3.7 \pm 0.3) \times 10^6$ s^{-1} was found for k_F, whereas k_{NR} was equal to $(1.5 \pm 0.3) \times 10^6$ s^{-1}.

4.2. Fluorescence Measurements of PROBE as a Function of Added Quaternary Ammonium Salt. An increase in the PROBE concentration automatically induces a change in two important parameters, namely, the salt concentration (which is relevant to the ion aggregation) and the pyrene concentration (which is relevant to the excimer formation). One way to study the salt influence on the probe behavior is to add a simple quaternary ammonium salt to the solution. Solutions of the reference probe, 1-methylpyrene, were prepared at a low concentration (1×10^{-6} M) and with increasing concentrations of t-BUTAP. The concentration range of the added salt extended from 1×10^{-4} M to 2×10^{-3} M. Solutions of PROBE were prepared in an analogous way. The added salt in this case was DOTAP (2×10^{-6} M PROBE, 2×10^{-3} M, 1×10^{-3} M, 5×10^{-4} M, and 1×10^{-4} M DOTAP).

SCHEME 3

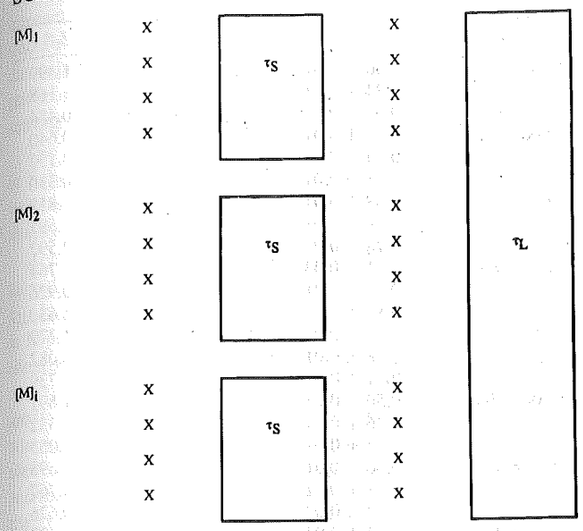

4.2.1. Stationary Measurements. The fluorescence emission spectra of PROBE did not change upon adding DOTAP to the solution (Figure not shown).

4.2.2. Time-Resolved Measurements. For PROBE and 1-methylpyrene two timing calibrations were used in the fluorescence decay measurements: 1.204 ns/channel and 121 ps/channel. All decay data of 1-methylpyrene could be described in standard global analysis by a monoexponential function (eq 36 with $n = 1$) with the decay time linked over the different t-BUTAP concentrations. This means that the addition of t-BUTAP does not influence the kinetic and spectroscopic behavior of 1-methylpyrene.

The decay data of PROBE in the presence of DOTAP could not be described by a monoexponential function: a biexponential decay function (eq 36 with $n = 2$) was needed to get satisfactory statistics of the fits.

$$f(\lambda^{em},\lambda^{ex},t) = \sum_{i=1}^{n}\alpha_i \exp(-t/\tau_i) \qquad t \geq 0 \qquad (36)$$

One decay time was found to be independent of the salt concentration, because it could be linked over the data surface of several experiments performed at different salt concentrations. Scheme 3 represents the linking scheme applied in the analysis. In this scheme boxed parameters represent the linked decay times τ_i, while X denotes the preexponential factors α_i. The long decay time τ_L was linked over all the decays at different salt concentrations and recorded at different wavelengths, whilst the short decay time τ_S was linked over experiments at each concentration at different wavelengths. Table 1 shows the decay parameters estimated by standard global biexponential analysis. For an intermolecular two-state excited-state process, there are only two cases where one of the decay times can be independent of the concentration. These are discussed in the Appendix. Since k_{01} is known and a shorter decay time appears upon addition of the salt, we have that $k_{01} = k_{02}$.

The 24 curves which were fitted by standard global biexponential analysis were subsequently analyzed in a single step by global compartmental analysis (Scheme 4). Since the fluorescence was recorded at three emission wavelengths and four

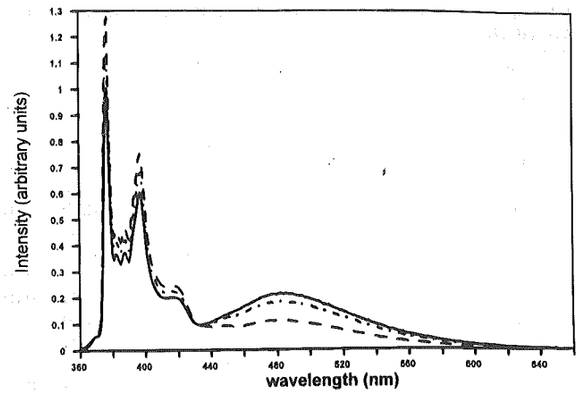

Figure 8. Emission spectra (normalized at 377 nm) of PROBE at 1×10^{-3} M (full line), 6×10^{-4} M (dotted line), and 4×10^{-4} M (dahed line) in THF.

SCHEME 4

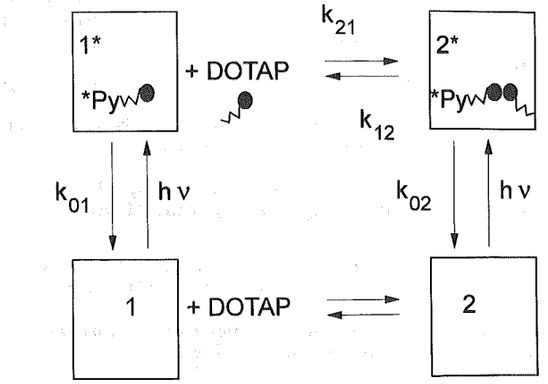

different salt concentrations, the compartmental system[31] is theoretically identifiable.[19] During the analysis the rate constants (k_{01}, k_{21}, k_{02}, and k_{12}) were linked over the whole fluorescence decay surface, the $\tilde{b}_1$ parameters were linked at the same [DOTAP], while the $\tilde{c}_1$ parameters were linked at the same λ^{em}. In Tables 2 and 3 the values for the decay parameters obtained by this analysis are shown. The results confirm that k_{01} and k_{02} are equal.

Defining $K^* = k_{21}/k_{12}$, the value obtained for this constant is 700 ± 130 M^{-1}. The constant K^* describes the dipole−dipole/ion−dipole association between the quaternary ammonium salts of excited PROBE and DOTAP.

The value of K^* is similar to the values obtained for this association in the ground-state obtained by vapor pressure osmometry and conductometric experiments.[32] Since the value of K^* lies in the same region, the excitation of the pyrene chromophore does not seem to exert an influence on the association.

4.3. The Properties of PROBE as a Function of Its Concentration. The fluorescence measurements were done on solutions with 1×10^{-3}, 8×10^{-4}, 6×10^{-4}, 4×10^{-4}, 2×10^{-4}, 1×10^{-4}, and 6×10^{-5} M PROBE in THF.

4.3.1. Stationary Measurements. Upon increase of the concentration of PROBE an additional fluorescence band occurs at longer wavelength (see Figure 8). This emission band with a maximum at 480 nm is due to excimer emission.

4.3.2. Time-Resolved Measurements. At each PROBE concentration the solutions were measured at six different emission wavelengths and at three time increments: 1.628, 0.804, and 0.218 ns/channel. At each PROBE concentration the decays were analyzed simultaneously by standard global

TABLE 1: Globally Estimated Decay Parameters of PROBE (2×10^{-6} M) in THF as a Function of the Concentration of Added DOTAP[a]

λ^{em} (mm)	[DOTAP] (M)	t_i (ns/ch)	α_S	τ_S (ns)	α_T	τ_T (ns)	Z_{χ^2}[b]
400	1×10^{-4}	1.208	-0.01 ± 0.01	13.5 ± 0.01	0.90 ± 0.01	223.3 ± 0.1	1.399
405			-0.01 ± 0.01		0.84 ± 0.01		1.168
410			-0.02 ± 0.01		0.93 ± 0.01		−0.484
400	5×10^{-4}		-0.02 ± 0.01	12.06 ± 0.01	0.79 ± 0.01		0.640
405			-0.02 ± 0.01		0.84 ± 0.01		0.150
410			0.00 ± 0.01		0.88 ± 0.01		−0.330
400	1×10^{-3}		-0.06 ± 0.01	9.9 ± 0.4	0.88 ± 0.01		0.812
405			0.00 ± 0.01		0.79 ± 0.01		0.691
410			0.01 ± 0.01		0.78 ± 0.02		2.592
400	2×10^{-3}		-0.04 ± 0.01	11.5 ± 0.6	0.91 ± 0.03		2.764
405			-0.00 ± 0.01		0.79 ± 0.01		0.926
410			-0.01 ± 0.01		0.85 ± 0.02		−1.630
405	1×10^{-4}	0.121	0.06 ± 0.02	13.5 ± 0.01	0.54 ± 0.01		1.779
410			0.05 ± 0.01		0.48 ± 0.01		0.082
415			0.05 ± 0.01		0.51 ± 0.01		0.739
405	5×10^{-4}		0.06 ± 0.01	12.06 ± 0.01	0.50 ± 0.01		1.691
410			0.05 ± 0.01		0.46 ± 0.01		−0.332
415			0.06 ± 0.01		0.47 ± 0.01		0.055
405	1×10^{-3}		0.07 ± 0.01	9.9 ± 0.4	0.56 ± 0.01		2.698
410			0.07 ± 0.01		0.52 ± 0.01		0.767
415			0.07 ± 0.01		0.52 ± 0.02		0.626
405	2×10^{-3}		0.06 ± 0.01	11.5 ± 0.6	0.57 ± 0.03		0.629
410			0.06 ± 0.01		0.54 ± 0.01		0.654
415			0.06 ± 0.01		0.52 ± 0.02		−2.204

[a] Experiments were performed at two time increments per channel (t_i): 1208 and 121 ps. Excitation wavelength was at 320 nm. For the analysis of the 24 decays a $Z_{\chi_g^2}$ value of 4.515 was obtained.

TABLE 2: Rate Constant Values Estimated by Global Compartmental Analysis ($Z_{\chi_g^2} = 4.778$) of the 24 Decay Curves of Table 1

$k_{01} = (4.46 \pm 0.01) \times 10^6\ s^{-1}$ $k_{02} = (4.48 \pm 0.01) \times 10^6\ s^{-1}$
$k_{21} = (42 \pm 7) \times 10^9\ M^{-1}\ s^{-1}$ $k_{12} = (5.7 \pm 0.1) \times 10^7\ s^{-1}$

TABLE 3: Spectral Parameter Values Estimated by the Global Compartmental Analysis of Table 2

[DOTAP] (M)	$\tilde{b}_1$	λ^{em} (nm)	$\tilde{c}_1$
1×10^{-4}	0.94 ± 0.01	400	0.69 ± 0.02
		405	$0.64 + 0.02$
		410	0.66 ± 0.01
		415	0.71 ± 0.02
5×10^{-4}	0.75 ± 0.02	400	0.69 ± 0.02
		405	$0.64 + 0.02$
		410	0.66 ± 0.01
		415	0.71 ± 0.01
1×10^{-3}	0.73 ± 0.01	400	0.69 ± 0.02
		405	$0.64 + 0.02$
		410	0.66 ± 0.01
		415	0.71 ± 0.02
2×10^{-3}	0.65 ± 0.01	400	0.69 ± 0.02
		405	$0.64 + 0.02$
		410	0.66 ± 0.01
		415	0.71 ± 0.02

triple-exponential analysis with linked decay times. This implies a compartmental system with three excited-state species. The estimated decay times as a function of concentration are shown in Figure 9, indicating that the longest decay time decreases with increasing concentration.

The decay traces collected in the region where only the monomer emits (375 nm) can be described by a biexponential decay function. A triple-exponential function (eq 36 with $n = 3$) with two negative preexponential factors (rise times) and one positive preexponential factor (decay time) can be fitted to the data recorded in the region where only excimer emission is observed (520 nm). The sum of the three preexponential factors equals 0. From these observations it can be concluded that there are two monomer excited states and one excimer excited state. A possible physical model will have to include the ion aggregation of quaternary ammonium salts in THF. This has been investigated in the previous section and by conductometry[32]

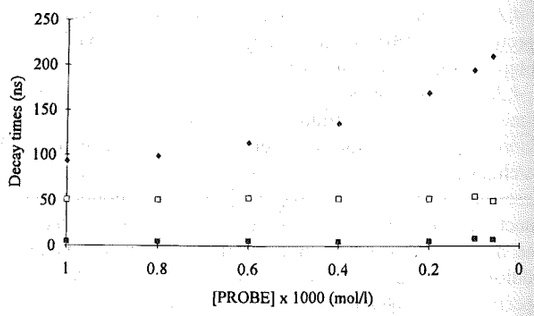

Figure 9. Decay times of PROBE as a function of the concentration in THF.

SCHEME 5

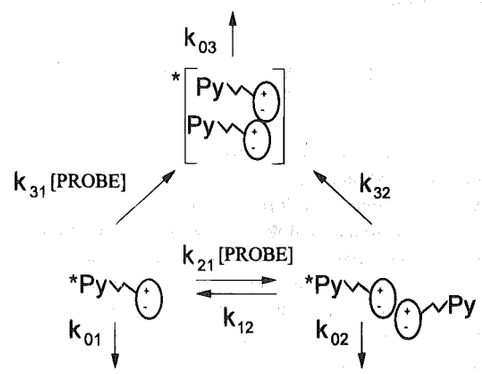

and vapor pressure osmometry.[31] Since the decay traces collected in the region where only the monomer emits (375 nm) can be described by a biexponential decay function, no excimer dissociation will occur during its lifetime. This means that k_{12} and k_{13} are both equal to 0. On the basis of these arguments the model depicted in Scheme 5 can be proposed.

The compartmental matrix corresponding to Scheme 5 is given by eq 7. The kinetics and identifiability have been treated in sections 2.1 and 2.2.

The transition between compartment one and compartment

two is an association phenomenon either due to ion−dipole interactions leading to triple ions or due to dipole−dipole interactions. It was previously found that for PROBE in THF the values of k_{01} and k_{02} are equal. This means that the same rate constant can be used in the linking scheme enabling the setting of limits on the other rate constants.

The identifiability study of the compartmental system depicted in Scheme 5 indicated that k_{01} and k_{03} can be determined in a unique way. Therefore, k_{01} and k_{03} were not kept constant during the analysis.

According to the identifiability study in section 2.1, the knowledge of k_{01}, k_{02}, and k_{03} allows one to specify limits on k_{21}, k_{31}, k_{12}, k_{32} (eqs 30−33). If one of these four rate constants is kept constant at a certain preset value, the system becomes identifiable. In practice, to determine the intervals of the rate constants k_{21}, k_{31}, k_{12}, and k_{32}, series of global compartmental analyses were performed in which one of those rate constants was kept constant at different preset values. All other parameters were freely adjustable. This procedure is referred to as *scanning*.[23] Values for A, B^*, and C^* (eqs 16, 28, and 29) can then be calculated, from which the bounds on the rate constants can be set. Figure 10a depicts the goodness-of-fit parameter $Z_{\chi_g^2}$ as a function of the scanned rate constant k_{31}. Using the estimated values of the rate constants, A (eq 16), B^* (eq 28), and C^* (eq 29) can be calculated and are depicted in Figure 10b−d. From visual inspection it is evident that an acceptable fit is obtained for $k_{31} < 5 \times 10^9\ M^{-1}\ s^{-1}$ (Figure 10a). Furthermore, note that in that region A, B^*, and C^* (Figure 10b−d) remain constant. Using the values of A ($(60 \pm 6) \times 10^9\ M^{-1}\ s^{-1}$), B^* ($(0.17 \pm 0.01) \times 10^9\ s^{-1}$), and C^* ($(9 \pm 1) \times 10^{18}\ M^{-1}\ s^{-2}$), the following bounds on the rate constants were calculated: $k_{31} < 7 \times 10^9\ M^{-1}\ s^{-1}$, $53 \times 10^9 < k_{21} < 60 \times 10^9\ M^{-1}\ s^{-1}$, $0.15 \times 10^9 < k_{12} < 0.17 \times 10^9\ s^{-1}$, and $k_{32} < 0.02 \times 10^9\ s^{-1}$. The values obtained for the other rate constants are $k_{01} = k_{02} = (4.25 \pm 0.01) \times 10^6\ s^{-1}$ and $k_{03} = (1.92 \pm 0.03) \times 10^7\ s^{-1}$. The obtained limits are independent of which rate constant is being scanned. If, for example, k_{21} is scanned, the region where $Z_{\chi_g^2}$ is minimal corresponds to the limits ($52 \times 10^9 < k_{21} < 60 \times 10^9\ M^{-1}\ s^{-1}$) found when k_{31} is scanned (Figure 11).

Do the obtained values of the rate constants and their bounds have a physical meaning? Using the value of k_{03} ($(1.92 \pm 0.03) \times 10^7\ s^{-1}$) estimated by global compartmental analysis, an excimer lifetime of 52 ± 1 ns is calculated. The excimer lifetimes of pyrene compounds at ambient temperature in similar solvents are known to be approximately 50 ns.[34]

The rate constants k_{21} and k_{12} are related to dipole−dipole and/or ion−dipole association/dissociation. As mentioned before, the association constants in ground (K) and excited (K^*) states are on the same order of magnitude. The limits on K^* calculated from $k_{21}^{min}/k_{12}^{max} < K^* < k_{21}^{max}/k_{12}^{min}$ are found to be $312 < K^* < 400\ M^{-1}$. Comparing these results with results obtained from addition of DOTAP (section 4.2) and the aggregation of quaternary ammonium salts in chloroform,[33] the obtained value has the right order of magnitude for ion−dipole or dipole−dipole interactions.

The rate constant k_{32} describes the intramolecular excimer formation within a dipole−dipole dimer or ion−dipole triple ion. The value lies within the range of values obtained by Reynders[35] in a study of the intramolecular excimer formation of bipyrenylalkanes.

The rate constant k_{31} is connected to the diffusion-controlled excimer formation. To obtain information about this process, the time-resolved emission of PROBE was measured in methanol. In this solvent PROBE does not aggregate, and an increase of its concentration results solely in the diffusion-

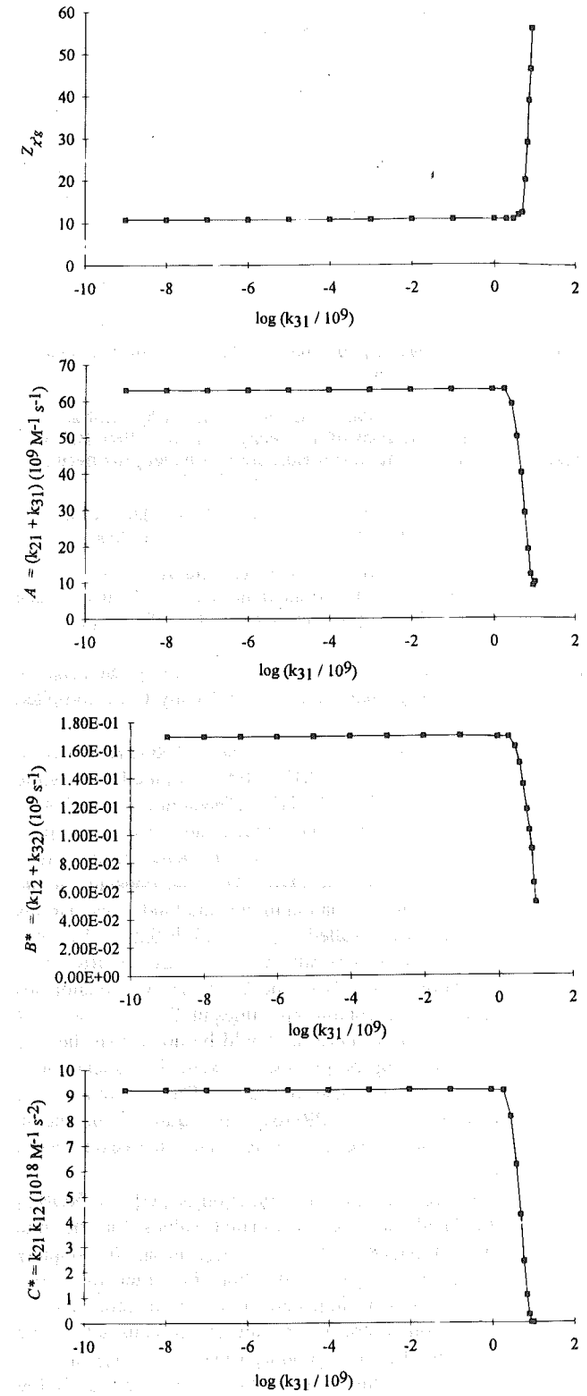

Figure 10. Global compartmental analysis of 99 decay traces of PROBE in THF collected at six emission wavelengths between 375 and 500 nm. Seven different PROBE concentrations were used: 1×10^{-3}, 8×10^{-4}, 6×10^{-4}, 4×10^{-4}, 2×10^{-4}, 1×10^{-4}, and 6×10^{-5} M at three different timing calibrations. (a) $Z_{\chi_g^2}$ values (eq 35) as a function of $\log(k_{31}/10^9)$. (b) A values (eq 16) calculated from the scanned k_{31} values and the estimated k_{21} values as a function of $\log(k_{31}/10^9)$. (c) B^* values (eq 28) calculated from the estimated k_{31} and k_{32} values as a function of $\log(k_{31}/10^9)$. (d) C^* values (eq 29) calculated from the k_{12} and k_{21} values as a function $\log(k_{31}/10^9)$.

controlled formation of excimers. Indeed the decay of the PROBE emission in methanol was found to be monoexponential at very low concentrations and biexponential at higher concentrations. A bicompartmental scheme similar to that described

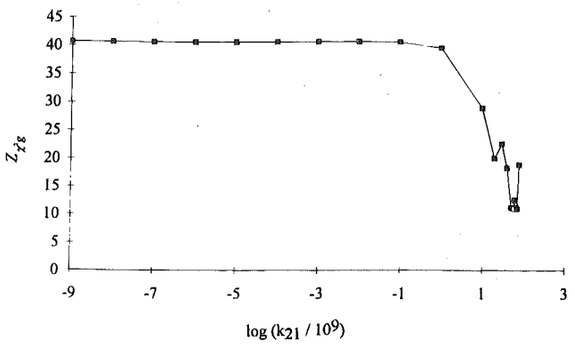

Figure 11. $Z_{\chi_g}^2$ values (eq 16) from a global compartmental analysis as a function of $\log(k_{31}/10^9)$.

TABLE 4: Rate Constant Values Estimated by Global Compartmental Analysis of 17 Decay Traces of PROBE in Methanol Collected at Seven Emission Wavelengths between 380 and 500 nm[a]

$k_{01} = (3.81 \pm 0.01) \times 10^6\ s^{-1}$	$k_{02} = (1.95 \pm 0.01) \times 10^7\ s^{-1}$
$k_{21} = (1.3 \pm 0.2) \times 10^9\ M^{-1}\ s^{-1}$	$k_{12} = (1 \pm 3) \times 10^4\ s^{-1}$

[a] Three different PROBE concentrations were used: 1.5×10^{-3}, 5×10^{-4}, and 1×10^{-5} M at two different timing calibrations: 1.204 and 0.121 ns/ch. The analysis gave a value of 0.158 for $Z_{\chi^2 g}$.

in the Appendix was constructed, and the resulting rate constant values estimated by global compartmental analysis are compiled in Table 4.

It can be concluded that the k_{01} value of PROBE is solvent dependent as $k_{01} = (3.81 \pm 0.01) \times 10^6\ s^{-1}$ in methanol, while $k_{01} = (4.2 \pm 0.1) \times 10^6\ s^{-1}$ in THF. The sum of the radiative and nonradiative decays of the excimer are solvent independent: $k_{02} = (1.95 \pm 0.01) \times 10^7\ s^{-1}$ in methanol and $k_{03} = (1.96 \pm 0.07) \times 10^7\ s^{-1}$ in THF. The rate constant of the intermolecular excimer formation in methanol indicates that this process is diffusion controlled: $k_{21} = (1.3 \pm 0.2) \times 10^9\ M^{-1}\ s^{-1}$. Since the methanol viscosity at 20 °C does not differ from that of THF (both 0.55 mPa s), the k_{21} value in methanol lies within the range of acceptable k_{31} values in THF: $0 < k_{31} < 7 \times 10^9\ M^{-1}\ s^{-1}$. Furthermore, it should be noted that the rate constant k_{12} describing the process of excimer dissociation in methanol is 0. This was also the case in THF where $k_{13} = 0$. Since $\tilde{b}_1$ equals unity at each PROBE concentration in methanol, there are no ground-state dimers which give rise to excimers in this solvent.

Finally, the decay times τ_i as a function of [M] = [PROBE] can be calculated using the estimated values for the rate constants and [M] (eqs 8−11). For k_{01}, k_{02}, and k_{03} the uniquely determined values can be used. For the other rate constants—which are known within certain limits—an arbitrary value of k_{31} in the region where A, B^*, and C^* are constant can be used together with the corresponding values of k_{21}, k_{12}, and k_{32}. The calculated decay times are plotted as a function of -log [PROBE] (Figure 12). The decay times estimated by standard global triple-exponential analysis are also shown in this figure and agree perfectly with those obtained through global compartmental analysis. The τ_i vs −log plots show the behavior typical for type B class 2 (section 2.1, Figure 4b), as is expected from the obtained values of k_{ij}.

5. Conclusions

The covalent linking of a quaternary ammonium salt exerts an influence on the pyrene moiety. This is proven by comparison of the data from the time-resolved fluorescence measurements of PROBE with the corresponding data of a reference probe, 1-methylpyrene. At very low concentrations

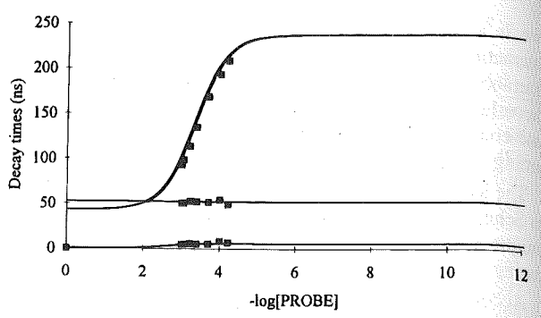

Figure 12. Decay times as a function of −log [M] calculated with the estimated values for the rate constants. For k_{01}, k_{02}, and k_{03} the uniquely determined values were used. For the other rate constants an arbitrary value of k_{31} was used together with the corresponding values of k_{21}, k_{12}, and k_{32}. The decay times estimated by the global triple-exponential analysis are also shown.

PROBE decays monoexponentially, with $k_{01} = (4.2 \pm 0.1) \times 10^6\ s^{-1}$, whereas k_{01} of 1-methylpyrene equals $(5.2 \pm 0.1) \times 10^6\ s^{-1}$.

Upon increase of the quaternary ammonium salt concentration an association occurs due to ion−dipole or dipole−dipole interactions. A biexponential decay is needed to fit the data. A bicompartmental scheme can be presented describing these processes. The rate constant values describing the kinetic scheme were obtained by global bicompartmental analysis: $k_{01} = k_{02}$, $k_{21} = (42 \pm 7) \times 10^9\ M^{-1}\ s^{-1}$, and $k_{12} = (5.7 \pm 0.1) \times 10^7\ s^{-1}$.

Increase of the PROBE concentration, so that pyrene moiety and salt concentration increase simultaneously, leads to a triple-exponential decay. Three excited-state species are present, and a kinetic scheme describing the processes between the three compartments is proposed (Scheme 5). To obtain information from the fluorescence decay surface, we developed global tricompartmental analysis. Even after including the information available from experiments where DOTAP was added ($k_{01} = k_{02}$), and the information available from the global triple-exponential analysis ($k_{13} = 0$ and $k_{23} = 0$), the experimental time-resolved data do not allow one to obtain a unique solution for the rate constant values. By applying the scanning technique, upper and lower bounds could be specified for the rate constants: $53 \times 10^9 < k_{21} < 60 \times 10^9\ M^{-1}\ s^{-1}$, $k_{31} < 7 \times 10^9\ M^{-1}\ s^{-1}$, $1.5 \times 10^8 < k_{12} < 1.7 \times 10^8\ s^{-1}$, and $k_{32} < 2 \times 10^7\ s^{-1}$. The maximum value of the rate constant of excimer formation, k_{31}, is much lower than the value of the rate constant k_{21}, which describes the aggregation. The values of k_{21} and k_{12} of the tricompartmental system can be compared with those of the bicompartmental system with DOTAP as added salt. Unique values were obtained for k_{01}, k_{02}, and k_{03}: $k_{01} = k_{02} = (4.25 \pm 0.01) \times 10^7\ s^{-1}$; $k_{03} = (1.92 \pm 0.03) \times 10^7\ s^{-1}$.

Acknowledgment. B.H. thanks the IWONL for a predoctoral fellowship. N.B. is an Onderzoeksleider of the Belgian Fonds voor Geneeskundig Wetenschappelijk Onderzoek. Dr. Jan van Stam is thanked for discussions and critical reading of the text. The financial support of Dienst Wetenschapsbeleid DWTC through IUAP-III-040 is gratefully acknowledged.

6. Appendix

Consider a causal, linear, time-invariant, intermolecular system consisting of two distinct types of ground-state species (1, 2) and two corresponding excited-state species (1*, 2*), as depicted, for example, in Scheme 4. In that case the compartmental matrix **A** is given by eq A.1, where the rate constants have the same meaning as before.

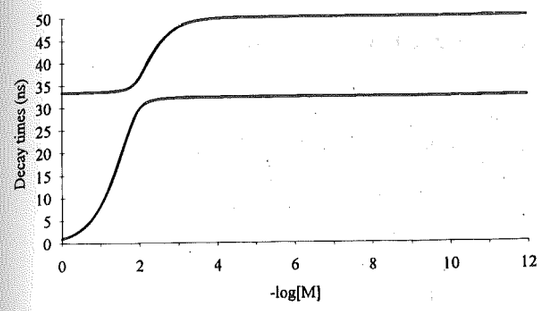

Figure 13. Decay times (eqs 8, A.2) as a function of −log [M] calculated with $k_{01} = 0.02 \times 10^9\ s^{-1}$, $k_{21} = 1 \times 10^9\ M^{-1}\ s^{-1}$, $k_{02} = 0.03 \times 10^9\ s^{-1}$, and $k_{12} = 0.001 \times 10^9\ s^{-1}$.

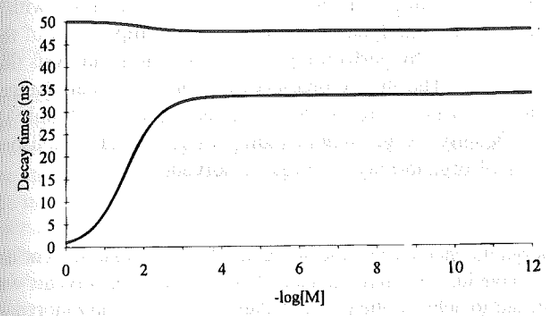

Figure 14. Decay times (eqs 8, A.2) as a function of −log [M] calculated with $k_{01} = 0.03 \times 10^9\ s^{-1}$, $k_{21} = 1 \times 10^9\ M^{-1}\ s^{-1}$, $k_{02} = 0.02 \times 10^9\ s^{-1}$, and $k_{12} = 0.001 \times 10^9\ s^{-1}$.

$$\mathbf{A} \equiv \begin{bmatrix} -(k_{01} + k_{21}[M]) & k_{12} \\ k_{21}[M] & -(k_{02} + k_{12}) \end{bmatrix} \quad \text{(A.1)}$$

The eigenvalues $\gamma_{1,2}$ of the bicompartmental system are related to the decay times according to eq 8 and are given by

$$\gamma_{1,2} = -{}^1/_2\{(X_1 + X_2) \mp [(X_1 - X_2)^2 + 4P[M]]^{1/2}\} \quad \text{(A.2)}$$

with

$$X_1 = k_{01} + k_{21}[\mathrm{M}] \quad \text{(A.3)}$$

$$X_2 = k_{02} + k_{12} \quad \text{(A.4)}$$

$$P = k_{21}k_{12} \quad \text{(A.5)}$$

We shall refer to the two decay times as τ_L and τ_S with $\tau_L > \tau_S$. To check which information can be obtained from a certain concentration range of [M], the two decay times can be plotted as a function of the concentration. At extremely low [M] the values of the decay times equal the values of $1/k_{01}$ and $1/(k_{02} + k_{12})$. At the high concentration end τ_S goes to 0 and τ_L reaches a value of $1/k_{02}$. Depending on the relative values of k_{01} and k_{02}, two classes can be distinguished.

Type A: $k_{01} \leq k_{02}$. At very low [M] τ_L equals $1/k_{01}$, whereas τ_S equals $1/(k_{02} + k_{12})$. At high [M] τ_L equals $1/k_{02}$, whereas

τ_S goes to 0. This is depicted in Figure 13. In this case τ_L will become independent of [M] if $k_{01} = k_{02}$.

Type B: $k_{02} < k_{01}$. At very low [M] τ_L equals $1/(k_{02} + k_{12})$, whereas τ_S equals $1/k_{01}$. At high [M] τ_L equals $1/k_{02}$, whereas τ_S goes to 0. This is depicted in Figure 14. In this case τ_L will become independent of [M] if k_{12} is negligible compared to k_{02}.

References and Notes

(1) Armstrong, R. W.; Strauss, U. P. *Encyclopedia of Polymer Science and Technology;* **1969**, *10*, 781.
(2) Bockris, J.; Reddy, A. *Modern Electrochemistry*; Plenum Press: New York, 1970.
(3) Lundberg, RD. *Structure and Properties of Ionomers;* Pineri M., Eisenberg A., Eds.; NATO ASI Series; D. Reidel: Dordrecht, 1987; pp 387−397.
(4) Hara, M.; Lee, A. H.; Wu, J. *J. Polym. Sci.: Part B: Polym. Phys.* **1987**, *25*, 1407−1418.
(5) Lantman, C. W.; MacKnight, W. J.; Peiffer, D. G.; Sinha, S. K.; Lundberg, R. D. *Macromolecules* **1987**, *20*, 1096−1101.
(6) Hara, M.; Wu, J.; Lee, A. *Macromolecules* **1988**, *21*, 2214−2218.
(7) Hara, M.; Wu, J.; Lee, A. *Macromolecules* **1989**, *22*, 754−757.
(8) Hara, M.; Wu, J. *Macromolecules* **1988**, *21*, 402−407.
(9) Lantman, C. W.; MacKnight, W. J.; Higgins, J. S.; Peiffer, D. G.; Sinha, S. K.; Lundberg, R. D. *Macromolecules* **1988**, *21*, 1339−1443.
(10) Gabrys, B.; Higgins, J. S.; Lantman, C. W.; MacKnight, W. J.; Pedley, A. M.; Peiffer, D. G.; Rennie, A. R. *Macromolecules* **1989**, *22*, 3746−3751.
(11) Pedley, A. M.; Higgins, J. S.; Peiffer, D. G.; Rennie, A. R. *Macromolecules* **1989**, *22*, 3746−3751.
(12) Broze, G.; Jérôme, R.; Teyssié, Ph. *Macromolecules* **1982**, *15*, 920−927.
(13) Broze, G.; Jérôme, R.; Teyssié, Ph. *Macromolecules* **1982**, *15*, 1300−1305.
(14) Broze, G.; Jérôme, R.; Teyssié, Ph.; Marco C. *Macromolecules* **1983**, *16*, 996−1000.
(15) Jérôme, R.; Broze, G.; Teyssié, Ph. *Microdomains in Polymer Solutions;* Dubin, P., Ed.; Plenum: New York, 1985; Polymer science and technology, Vol. 30, p 243.
(16) Jérôme, R. *Structure and Properties of Ionomers;* Pineri M., Eisenberg A., Eds.; NATO ASI Series; D. Reidel: Dordrecht, 1987; p 399.
(17) Jérôme, R.; Henrioulle-Granville, M.; Boutevin, B.; Robin, J. J. *Prog. Polym. Sci.* **1991**, *16*, 837−906.
(18) Granville, M.; Jérôme, R.; Teyssié, Ph.; De Schryver, F. C. *Macromolecules* **1988**, *21*, 2894−2896.
(19) Ameloot, M.; Boens, N.; Andriessen, R.; Van den Bergh, V.; De Schryver, F. C. *J. Phys. Chem.* **1991**, *95*, 2041.
(20) Beechem, J.; Ameloot, M.; Brand, L. *Chem. Phys. Lett.* **1985**, *120*, 466.
(21) Löfroth, J.-E. *Anal. Chem.* **1985**, *14*, 403.
(22) Löfroth, J.-E. *Eur. Biophys. J.* **1985**, *13*, 45.
(23) Van Dommelen, L.; Boens, N.; Ameloot, M.; De Schryver, F. C.; Kowalczyk, A. *J. Phys. Chem.* **1993**, *97*, 11738.
(24) Chabanel, M. *Pure Appl. Chem.* **1990**, *62*, 35.
(25) Boens, N.; Janssens, L.; De Schryver, F. C. *Biophys. Chem.* **1989**, *33*, 77.
(26) (a) Demas, J. N.; Crosby, G. A. *J. Phys. Chem.* **1971**, *75*, 991. (b) Morris, J. V.; Mahaney, M. A.; Huber, J. R. *J. Phys. Chem.* **1976**, *80*, 969.
(27) Marquardt, D. W. *J. Soc. Ind. Appl. Math.* **1963**, *11*, 431.
(28) Boens, N. In *Luminescence Techniques in Chemical and Biochemical Analysis*; Baeyens, W. R. G., De Keukeleire, D., Korkidis, K., Eds.; Marcel Dekker: New York, 1991; p 21.
(29) Viaene, K.; Verbeeck, A.; Gelade, E.; De Schryver, F. C. *Langmuir* **1986**, *2*, 456.
(30) Almgren, M.; Medhage, B.; Mukhtar, E. J. *Photochem. Photobiol. A: Chem.* **1991**, *59*, 325.
(31) Boens, N.; Van Dommelen, L.; Ameloot, M. *Biophys. Chem.* **1993**, *48*, 301.
(32) Czapkiewicz, J.; Maciejowska, I. *Colloids Surf.* **1992**, *63*, 323.
(33) Mukuri, P. K.; Hazra, D. K. J. *Chem. Soc. Trans.* **1991**, *21*, 3511.
(34) Lopez-Arbeloa, F. Doctoral thesis, K. U. Leuven, 1987.
(35) Reynders, P. Doctoral thesis, Göttingen, 1988.

JP942595O